CHEMISTRY OF MATERIALS
Article

Chem. Mater. **2010,** *22,* 5739–5746 5739
DOI:10.1021/cm101972h

Nanocasting of Ordered Mesoporous Co_3O_4-Based Polyoxometalate Composite Frameworks

Gerasimos S. Armatas,*[,†] Alexandros P. Katsoulidis,[‡] Dimitris E. Petrakis,[§] Philippos J. Pomonis,[§] and Mercouri G. Kanatzidis[‡]

[†]*Department of Materials Science and Technology, University of Crete, Heraklion 71003, Crete, Greece,* [‡]*Department of Chemistry, Northwestern University, Evanston, Illinois 60208, United States, and* [§]*Department of Chemistry, University of Ioannina, Ioannina 45110, Greece*

Received July 15, 2010. Revised Manuscript Received September 9, 2010

We report the synthesis of highly ordered mesoporous frameworks consisting of nanocrystalline Co_3O_4 and Keggin-type tungstophosphoric acid ($HPW_{12}O_{40}$, HPW) compounds using the hard-templating method. The resulting materials feature a Co_3O_4/HPW solid solution structure with different HPW loadings, i.e., 6, 11, 15, and 36 wt %. Characterization by small-angle X-ray scattering (SAXS), high-resolution transmission electron microscopy (TEM), and N_2 physisorption measurements reveal that all mesoporous frameworks possess a three-dimensional cubic symmetry with large internal Brumauer−Emmett−Teller (BET) surface area (87−141 m^2g^{-1}) and narrow sized pores (ca. 4 nm). The Keggin structure of the incorporated $PW_{12}O_{40}{}^{3-}$ clusters within the composite frameworks was confirmed with X-ray diffused scattering and atomic pair distribution function (PDF) analysis, X-ray photoelectron spectroscopy (XPS), infrared (IR), and diffuse-reflectance UV/vis spectroscopy. Catalytic studies have indicated that these Co_3O_4/HPW composites can be effective catalysts, exhibiting remarkable catalytic activity on direct decomposition of N_2O.

Introduction

Mesoporous nanocomposite structures of transition metal oxides with large internal surface area and uniform pores are of immense interest in many technological fields, including catalysis, magnetism, selective absorption, and separation.[1] These materials can combine complementary functionalities into the inorganic structure such as regular mesoporosity and high catalytic activity. Of particular interest is the design and synthesis of well-ordered metal oxide mesostructures that utilize structure-directing processes of "soft" organic surfactants or "hard" inorganic molds.[2] Although the direct liquid-crystal templating from amphiphilic surfactants has been successfully applied for mesoporous silicates, such as MCM-41 and SBA-15, the synthesis of mesoporous transition-metal oxides is challenging because of the redox instability and phase transition of metal-oxide structures after template removal.[3]

Nanocasting provides an alternative route for the fabrication of mesoporous metal oxides with controlled composition and textural topology.[4] This approach involves impregnation and inverse replica solidification of suitable inorganic precursors within the pore channels of a silica template. After etching the silica walls, the shape-reversed templated structure can easily be obtained as a product. Originally used for mesoporous carbon (CMK-type materials),[5] this method was been extended to mesoporous metals, such as Pt[6] and Ag[7] and transition-metal oxides, such as Co_3O_4,[8] Mn_xO_y,[8] Fe_2O_3,[9] Cr_2O_3,[10] NiO,[11] CuO,[12] WO_3,[13] CeO_2,[14] RuO_2,[15] and In_2O_3.[16]

*To whom correspondence should be addressed. E-mail: garmatas@materials.uoc.gr. Phone: +30-2810-545004. Fax: +30-2810-394273.

(1) (a) Carreon, M. A.; Guliants, V. V. *Eur. J. Inorg. Chem.* **2005**, 27. (b) Grosso, D.; Boissière, C.; Smarsly, B.; Brezesinski, T.; Pinna, N.; Albouy, P. A.; Amenitsch, H.; Antonietti, M.; Sanchez, C. *Nat. Mater.* **2004**, *3*, 787. (c) Yang, P.; Zhao, D.; Margolese, D. I.; Chmelka, B. F.; Stucky, G. D. *Chem. Mater.* **1999**, *11*, 2813. (d) Schüth, F.; Schmidt, W. *Adv. Eng. Mater.* **2002**, *4*, 269. (e) Garcia, C.; Zhang, Y. M.; DiSalvo, F.; Wiesner, U. *Angew. Chem., Int. Ed.* **2003**, *42*, 1526.
(2) (a) Yue, W.; Zhou, W. *Prog. Nat. Sci.* **2008**, *18*, 1329. (b) Corma, A. *Chem. Rev.* **1997**, *97*, 2373. (c) Lu, A.-H.; Schüth, F. *Adv. Mater.* **2006**, *18*, 1793.
(3) (a) Schüth, F. *Chem. Mater.* **2001**, *13*, 3184. (b) Soler-Illia, G. J. A.; Sanchez, C.; Lebeau, B.; Patarin, J. *Chem. Rev.* **2002**, *102*, 4093.
(4) Lu, A. H.; Schüth, F. *Adv. Mater.* **2006**, *18*, 1793.
(5) Ryoo, R.; Joo, S. H.; Jun, S. *J. Phys. Chem. B* **1999**, *103*, 7743.
(6) Sakamoto, Y.; Ohsuna, T.; Hiraga, K.; Terasaki, O.; Ko, C. H.; Shin, H. J.; Ryoo, R. *Angew. Chem., Int. Ed.* **2000**, *39*, 3107.
(7) (a) Han, Y.-J.; Kim, J. M.; Stucky, G. D. *Chem. Mater.* **2000**, *12*, 2068. (b) Shon, J.-K.; Kong, S. S.; Kim, J. M.; Ko, C. H.; Jin, M.; Lee, Y. Y.; Hwang, S. H.; Yoon, J. A.; Kim, J.-N. *Chem. Commun.* **2009**, *6*, 650.
(8) (a) Tian, B. Z.; Liu, X.; Solovyov, L.; Liu, Z.; Yang., H.; Zhang, Z.; Xie, S.; Zhang, F.; Tu, B.; Yu, C.; Terasaki, O.; Zhao, D. *J. Am. Chem. Soc.* **2004**, *126*, 865. (b) Wang, Y.; Yang, C. M.; Schmidt, W.; Spliethoff, B.; Bill, E.; Schüth, F. *Adv. Mater.* **2005**, *17*, 53.
(9) Tian, B. Z.; Liu, X. Y.; Yang, H. F.; Xie, S. H.; Yu, C. Z.; Tu, B.; Zhao, D. Y. *Adv. Mater.* **2003**, *15*, 1370.
(10) Jiao, K.; Zhang, B.; Yue, B.; Ren, Y.; Liu, S.; Yan, S.; Dickinson, C.; Zhou, W.; He, H. *Chem. Commun.* **2005**, *45*, 5618.
(11) Yue, W. B.; Zhou, W. Z. *Chem. Mater.* **2007**, *19*, 2359.
(12) Lai, X.; Li, X.; Geng, W.; Tu, J.; Li, J.; Qiuet, S. *Angew. Chem., Int. Ed.* **2007**, *46*, 738.
(13) Yue, B.; Tang, H.; Kong, Z.; Zhu, K.; Dickinson, C.; Zhou, W.; He, H. *Chem. Phys. Lett.* **2005**, *407*, 83.
(14) Laha, S.; Ryoo, R. *Chem. Commun.* **2003**, *17*, 2138.
(15) Shen, W.; Shi, J.; Chen, H.; Gu, J.; Zhu, Y.; Dong, X. *Chem. Lett.* **2005**, *34*, 390.

Published on Web 09/29/2010

These mesoporous replicas possess a well-ordered crystalline framework from hexagonal *p6mm* ordered nanorods, to cubic *Ia*$\bar{3}$*d* bicontinuous nanowires, to cubic *Fm*$\bar{3}$*m* or *Im*$\bar{3}$*m* interconnected spherical nanocages, derived from mesoporous silicas SBA-15, KIT-5, and FDU-12 or SBA-16 as hard templates, respectively.

Intending to fabricate advanced materials with desired emergent properties, we are interested in assembling multifunctional mesostructures using preorganized nanocomposites or clusters, such as the metal-oxide compounds and polyoxometalates. The polyoxometalates of the early transition metals (especially Mo, W, and V) comprise an exceptional subclass of anionic metal−oxygen compounds with fascinating properties, especially those in redox- and photocatalysis.[17] The enormous structural and compositional diversity of polyoxometalates offer great opportunities for this direction. Cobalt oxide (Co_3O_4) is an important material with useful technological applications in redox catalysis, magnetism, and energy storage.[18] Nanostructured arrays of Co_3O_4 with ordered mesostructure and high surface area may exhibit unusual properties such as quantum confinement and improved electron transfer and magnetic interactions. It is expected that coupling of these functional components into a mesoporous structure can provide complementary or enhanced physicochemical properties in the former. However, the synthesis of such complex materials is a great challenge because of the low processability of polyoxometalates into ordered mesostructures and their tendency for decomposition.

Herein, we report, for the first time, on the synthesis of periodically ordered mesoporous frameworks consisting of cobalt oxide and tungstophosphoric acid ($H_3PW_{12}O_{40}$, hereafter HPW) components through a hard-templating technique. These materials can incorporate different functionalities into the composite structure, such as mesoporosity and physicochemical characteristics of Co_3O_4 and HPW components. To assemble the Co_3O_4/HPW composites, we employed cubic mesoporous KIT-6 silica, where a network of high-interconnected enantiomeric pore channels in *Ia*$\bar{3}$*d* symmetry act as a template. A series of mesoporous materials with different loading of HPW in Co_3O_4-based framework was obtained after dissolution of the silica walls. The products have a three-dimensional cubic structure with large internal surface area and narrow distribution of pore sizes and exhibit outstanding catalytic activity in the direct decomposition of N_2O.

Experimental Section

Synthesis. High quality mesoporous cubic *Ia*$\bar{3}$*d* silica material was prepared according to the method reported by Kleitz et al.[19] In a typical preparation of mesoporous Co_3O_4 and Co_3O_4/HPW(w) composites, 0.2 g of KIT-6 (aged at 90 °C) was dispersed to clear solution of 465 mg (1.6 mmol) of $Co(NO_3)_2 \cdot 6H_2O$ (Aldrich) and $H_3PW_{12}O_{40} \cdot 26H_2O$ in 2 mL of ethanol, and the resulting mixture was vigorously stirred for 1 h at room temperature. After drying at 40 °C for 24 h to undergo ethanol evaporation, the resulting powder was heated at 200 °C for 10 h to decompose cobalt nitrate precursor. The impregnation and decomposition steps were repeated twice in order to achieve higher loadings, and the obtained material was calcined at 400 °C for 6 h in air to prepare crystalline cobalt oxide networks inside the KIT-6 channels. The silica template was completely removed with a 5 wt % HF aqueous solution at room temperature. The black material was collected by filtration, washed with water and ethanol several times in order to remove silicon hydroxyl species (i.e., $Si(OH)_4$ or polymers), excess HF, and hydrofluorosilic acid byproducts, and dried at 80 °C for 24 h. Different Co_3O_4/HPW(w) mesostructures (where w refers to the weight percentage of $H_3PW_{12}O_{40}$ loading in the composite framework, i.e., w = 6, 11, 15, and 36 wt %) were obtained using 10, 20, 28, or 87 mg of $H_3PW_{12}O_{40} \cdot 26H_2O$, respectively. Nanostructured cobalt oxide material was also prepared following the above process in the absence of tungstophosphoric acid.

Catalytic Decomposition of N_2O. The N_2O decomposition was carried out in a bench-scale plug-flow reactor (PFR) connected with a gas chromatograph for analysis.[20] A gaseous mixture of N_2O (10 vol.%) in He was allowed to flow (60 mL min^{-1}) through the reactor, consisting of a silica tube 1 cm in diameter with a perforated glass bed on which 100 mg of sample was placed. The system was heated in a tubular furnace equipped with a temperature controller that holds the temperature within ±1 °C. The catalytic experiments were carried out from 250 to 400 °C, a temperature range where the catalysts are stable. Analyses of the reactants and products were carried out by sampling 1 mL of the gases to a PC-operated Shimadzu GC-15A equipped with a TCD, with He as carrier gas. The column used for analysis was a 2 m × 1/8 in., stainless steel containing a 5A molecular sieve.

Physical Characterization. Small-angle X-ray scattering (SAXS) patterns were collected on a Rigaku S-MAX 3000 high-brilliance system equipped with a two-dimensional wire detector and a Cu (λ = 1.54098 Å) rotating anode operated at 80 kV and 40 mA ($0.01 < q < 0.6$ $Å^{-1}$). Measurements were performed by transmission in samples that were gently grounded and held in a quartz capillary tube (I.D. 1 mm). The sample to detector distance and the center of the beam were precisely determined by calibration with a Ag-behenate diffraction standard (d_{001} = 58.38 Å). The diffraction intensities of two-dimensional collected images were integrated to yield one-dimensional diffraction patterns as a function of 2θ degrees with the FIT2D program.[21] Scattering data were corrected for dark current and empty tube scattering.

Nitrogen adsorption−desorption isotherms were measured at 77 K on a Micromeritics TriStar II 3020 sorption analyzer. Before the measurements were taken, the samples were outgassed at 150 °C under vacuum ($< 10^{-5}$ Torr) for 12 h. The specific surface areas were calculated using the Brumauer−Emmett−Teller (BET)[22] method on the adsorption data in the relative

(16) Yang, H.; Shi, Q.; Tian, B.; Lu, Q.; Gao, F.; Xie, S.; Fan, J.; Yu, C.; Tu, B.; Zhao, D. *J. Am. Chem. Soc.* **2003**, *125*, 4724.
(17) (a) Mizuno, N.; Misono., M. *Chem. Rev.* **1998**, *98*, 199. (b) Katsoulis., D. E. *Chem. Rev.* **1998**, *98*, 359.
(18) (a) Natile, M. M.; Glisenti, A. *Chem. Mater.* **2002**, *14*, 3090. (b) Wang, Y.; Yang, C.-M.; Schmidt, W.; Spliethoff, B.; Bill, E.; Schüth, F. *Adv. Mater.* **2005**, *17*, 53. (c) Fu, L.; Liu, Z.; Liu, Y.; Han, B.; Hu, P.; Cao, L.; Zhu, D. *Adv. Mater.* **2005**, *17*, 217. (d) Poizot, P.; Laruelle, S.; Grugeon, S.; Dupont, L.; Tarascon, J. M. *Nature* **2000**, *407*, 496.
(19) Kleitz, F.; Choi, S. H.; Ryoo, R. *Chem. Commun.* **2003**, *17*, 2136.
(20) (a) Loukatzikou, L. A.; Sdoukos, A. T.; Pomonis, P. J. *J. Mater. Chem.* **1997**, *7*, 1587. (b) Ladavos, A. K.; Giannakas, A. E.; Bakas, T. V.; Pomonis, P. J. *J. Catal.* **2007**, *251*, 103. (c) Petrakis, D. E.; Pomonis, P. J.; Sdoukos, A. T. *J. Chem. Soc. Faraday Trans. I* **1989**, *85*, 3173.
(21) Hammersley, A. P. *FIT2D: An Introduction and Overview*; ESRF Internal Report, ESRF97HA02T: Grenoble, France, 1997.
(22) Brunauer, S.; Deming, L. S.; Deming, W. S.; Teller, E. *J. Am. Chem. Soc.* **1940**, *62*, 1723.

pressure range of 0.05−0.26. The total pore volumes were estimated from the adsorbed amount at the relative pressure of $P/P_o = 0.98$, and the pore size distributions were obtained from the adsorption branch of the isotherms using the Barrett−Joyner−Halenda (BJH)[23] method.

Transmission electron micrographs (TEM) were recorded with a JEOL JEM-2100 electron microscope equipped with LaB_6 filament and operating at 200 kV. The samples were first gently ground, suspended in ethanol, and then picked up on a Cu grid covered with carbon film.

Quantitative microprobe analyses were performed on a JEOL JSM-6390LV scanning electron microscope (SEM) equipped with an Oxford INCA PentaFET-x3 energy dispersive X-ray spectroscopy (EDS) detector. Data acquisition was performed with an accelerating voltage of 20 kV and 60 s accumulation time.

The wide-angle X-ray diffraction analysis (XRD) data were recorded on an Inel X-ray diffractometer (40 KV, 20 mA) equipped with Ni-filtered Cu Kα radiation ($\lambda = 1.5405$ Å) in Debye−Scherrer geometry.

X-ray photoelectron spectroscopy was performed on an Omicron ESCA system equipped with a monochromated Al Kα X-ray (1486.6 eV) source with a 1.5 mm beam diameter and operated at 300 W. A low-energy electron flood gun was employed for charge neutralization. Samples were analyzed at pressure below 2×10^{-8} Torr with a pass energy of 25 eV and a takeoff angle of 45°. All binding energies were calibrated using the C 1s carbon peak (284.6 eV). Prior to X-ray photoelectron spectroscopy (XPS) measurement, the powders were pressed to form a pellet, and then, the pellet was put into the entry-load chamber to pump for 2 h. The relative atomic composition was determined from acquired spectra after background subtraction (linear type) by integrating the Co $2p_{3/2}$ and W $4f_{7/2}$ peaks and dividing by its sensitivity factor. The sensitivity factors of Co $2p_{3/2}$ (10) and W $4f_{7/2}$ (5.75) signals are provided by spectral data processor (SDP) software v4.3.

X-ray scattering data were recorded using high-energy synchrotron radiation (90.48 KeV, $\lambda = 0.13702$ Å) at the Advanced Photon Source (APS) at Argonne National Laboratory. The PDF plots $G(r)$ as a function of the interatomic distance r were obtained using the PDFFIT program.[24] The calculated PDF plots of models were calculated with the DISCUS[25] and PDFFIT programs.

Infrared spectra of solid samples were obtained on a Thermo Nicolet 6700 FT-IR spectrometer. Spectra were obtained on fine powders in diffused reflectance (DRIFT) mode under nitrogen atmosphere and averaging 254 interferograms with resolution of 2 cm^{-1}.

UV/vis diffuse reflectance spectra were recorded at room temperature with a Shimadzu model UV-3101PC double-beam, double monochromator spectrophotometer, using powder $BaSO_4$ as a 100% reflectance standard. Reflectance data were converted to absorption (α/S) date according to the Kubelka−Munk equation: $\alpha/S = (1 - R)^2/(2R)$, where R is the reflectance and α and S are the absorption and scattering coefficients, respectively.

Results and Discussion

Structural and Physical Properties. The chemical composition of template-free mesoporous materials was determined with energy-dispersive X-ray spectroscopy (EDS). The EDS spectra display strong signals from Co and W elements without detection of Si. The acquired atomic ratios of Co/W are consistent with a 6, 11, 15, and 36 wt % of HPW loading (w) in composite Co_3O_4/HPW(w) structures, which are very close to the nominal compositions (Table 1). This suggests complete incorporation of HPW clusters into the nanochannels of the silica template as well as minimal leaching of HPW upon etching the silica walls with HF solution. The absence of silicon suggests the complete dissolution of the silica mold (Figure S3, Supporting Information).

Table 1. Analytical Data of Mesoporous Co_3O_4/HPW(w) Composite Materials

sample	atomic ratio[a] (Co/P/W)	HPW loading (wt %)
Co_3O_4/HPW(6)	584.7:1.1:12	5.8
Co_3O_4/HPW(11)	300.2:1.1:12	10.7
Co_3O_4/HPW(15)	200.8:1.2:12	15.2
Co_3O_4/HPW(36)	63.6:1.1:12	36.1

[a] EDS elemental data normalized to the 12-atom W_{12} unit.

Figure 1 shows the small-angle X-ray scattering (SAXS) patterns of mesoporous Co_3O_4 and Co_3O_4/HPW(w) composite materials. The SAXS patterns display three well-resolved diffraction peaks at low 2θ scattering angles of 0.5−1.2° with q-vector ($=4\pi\cdot\sin\theta/\lambda$) value ratios of $1:(3)^{1/2}:(4)^{1/2}$, which can be indexed as 110, 211, and 220 Bragg reflections of cubic symmetry. The presence of 110 diffraction peaks suggests possible structure transformation from cubic $Ia\bar{3}d$ to $I4_132$ or lower space group symmetry after template removal.[26] The lowering of symmetry can be ascribed to the incomplete interconnection between the two enantiomeric gyroidal $Ia\bar{3}d$ subframeworks. On the basis of cubic symmetry and SAXS data, the lattice parameter (a_o) of mesoporous samples was estimated from the d-spacing of the 211 diffraction peak (see Table 2). These lattice parameters indicate a small structural shrinkage of ∼6.1−6.9% for mesoporous replicas relative to the silica template ($a_o = 23.1$ nm), possibly due to the low volume conversion from cobalt nitrate (density ∼ 1.9 g/cm^3) to cobalt oxide (density ∼ 6.1 g/cm^3).

The wide-angle XRD patterns of the mesoporous Co_3O_4 and Co_3O_4/HPW(w) composites showed several broad Bragg diffraction peaks, suggesting nanocrystalline Co_3O_4 (Figure 2). All the diffraction peaks can be indexed to the face-centered cubic $Fd\bar{3}m$ symmetry of spinel-type Co_3O_4 structure with lattice parameter $a_o = 0.8084$ nm (PDF no. 74-2120). The average crystallite size of the Co_3O_4 calculated from the peak-broadening of XRD using the Debye−Scherrer formula was found to be ∼8.8−9.4 nm. It can be observed that the increase in HPW loading resulted in a decrease in the coherent size of Co_3O_4 crystallite probably by inhibiting the growth of Co_3O_4 crystals during calcination. The size of these clusters is

(23) Barrett, E. P.; Joyner, L. G.; Halenda, P. H. *J. Am. Chem. Soc.* **1951**, *73*, 373.
(24) Proffen, T. H.; Billinge, S. J. L. *Appl. Cryst.* **1999**, *32*, 572.
(25) Proffen, T. H.; Neder, R. B. *J. Appl. Crystallogr.* **1997**, *30*, 171.
(26) (a) Solovyov, L. A.; Zaikovskii, V. I.; Shmakov, A. N.; Belousov, O. V.; Ryoo, R. *J. Phys. Chem. B* **2002**, *106*, 12198. (b) Kaneda, M.; Tsubakiyama, T.; Carlsson, A.; Sakamoto, Y.; Ohsuna, T.; Terasaki, O.; Joo, S. H.; Ryoo, R. *J. Phys. Chem. B* **2002**, *106*, 1256.

Table 2. Textural Properties of Mesoporous Co_3O_4 and Co_3O_4/HPW(w) Replicas Casted from KIT-6 Mesostructure (a_o = 23.1 nm)

material	surface area (m^2g^{-1})	pore volume[a] (cm^3g^{-1})	pore size (nm)	d_{211}-spacing (nm)	unit cell[b] (nm)	WT[c] (nm)	crystalline size[d] (nm)
Co_3O_4	141	0.25	4.1, 6.5	8.78	21.5	6.7	9.4
Co_3O_4/HPW(6)	119	0.29	4.0, 6.2	8.86	21.7	6.9	9.3
Co_3O_4/HPW(11)	120	0.22	3.9, 6.1	8.84	21.7	7.0	9.3
Co_3O_4/HPW(15)	109	0.31	3.8, 5.6	8.82	21.6	7.0	9.1
Co_3O_4/HPW(36)	87	0.26	3.9, 5.7	8.85	21.7	7.0	8.8

[a] Total pore volume at $P/P_o = 0.98$. [b] The unit cell parameter given by $\alpha_0 = d_{211}(6)^{1/2}$. [c] The framework wall thickness given by WT = $a_0/2 - D_p$, where D_p is the pore size. [d] The average crystalline size of Co_3O_4 calculated by the Debye–Scherrer formula $d_p = 0.9\lambda/B\cos\theta$, where λ is source wavelength ($\lambda_{cu} = 0.154$ nm) and B is the full-width half-maximum of the diffraction peak centered at 2θ degrees.

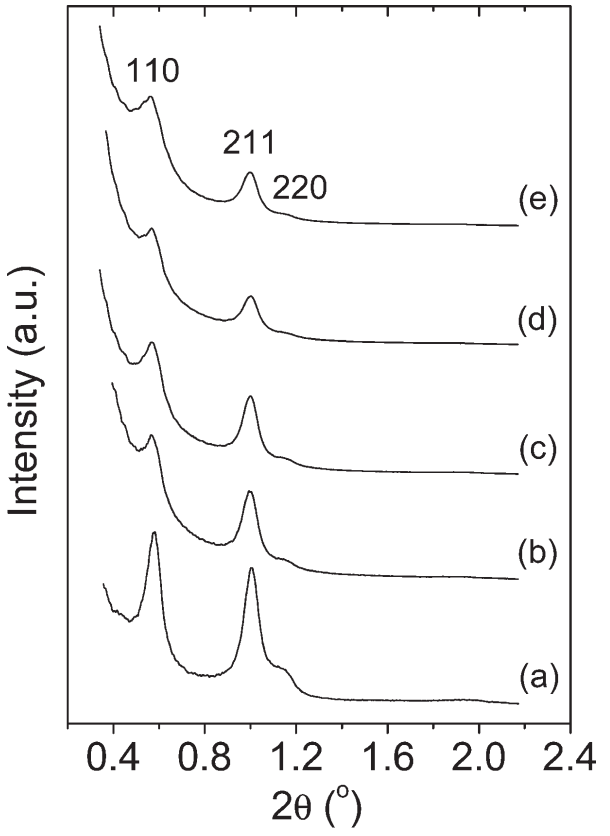

Figure 1. SAXS diffraction patterns of template-free mesoporous (a) Co_3O_4 and (b) Co_3O_4/HPW(6), (c) Co_3O_4/HPW(11), (d) Co_3O_4/HPW(15), and (e) Co_3O_4/HPW(36) composite materials.

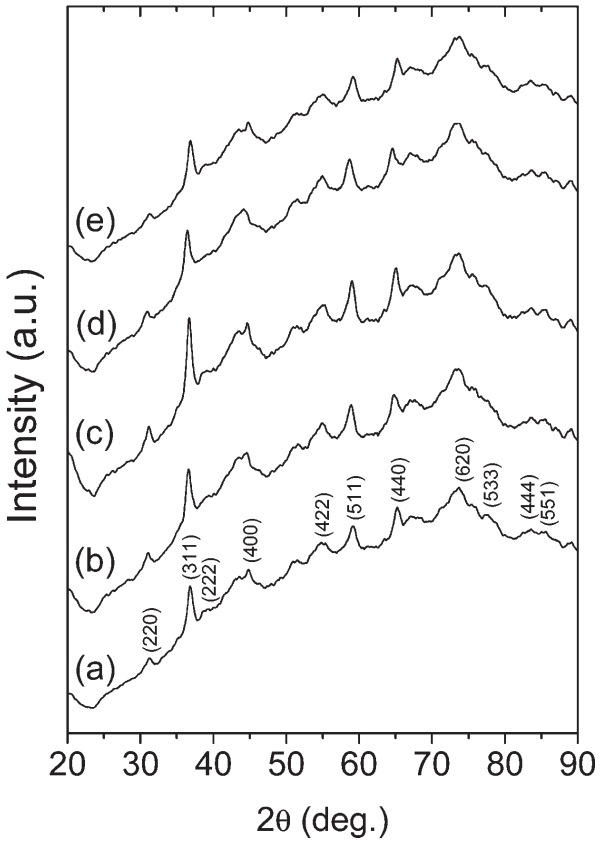

Figure 2. Wide-angle XRD patterns of mesoporous (a) Co_3O_4 and (b) Co_3O_4/HPW(6), (c) Co_3O_4/HPW(11), (d) Co_3O_4/HPW(15), and (e) Co_3O_4/HPW(36) composite materials. The indexing of the Bragg peaks is consisted with the face-centered cubic $Fd\bar{3}m$ unit cell with lattice parameter $a_o = 0.8084$ nm.

~1.2 nm, and by blending with the cobalt nitrate species can hinder the formation of extended Co_3O_4 crystalline structure inside the silica pores. However, these crystallite sizes are larger than the pore wall thickness of mesoporous replicas (see Table 2) and the pore diameter of the silica template (~8.2 nm, see Supporting Information). This can be understood if we consider an oriented growth of Co_3O_4 nanocrystals along the pore axis and the framework while the other direction (along the wall thickness) is much smaller. Note that the Debye–Scherrer analysis assumes spherical-shaped particles and gives an average size in all three dimensions. The absence of Bragg diffractions of the $H_3PW_{12}O_{40}$ in wide-angle XRD patterns indicates a homogeneous dispersion of molecular HPW clusters into the composite frameworks or the presence of too small amounts (<5wt %) of HPW crystallites in mesoporous structures.

Transmission electron microscopy (TEM) confirms that the replicas preserve the crystal structure of the silica template. Figure 3, shows typical TEM images and the corresponding fast-Fourier transform (FFT) patterns of mesoporous Co_3O_4/HPW(15), revealing a periodic arrangement of uniform nanowires in three-dimensional cubic symmetry. Analysis of the TEM images indicates an average pore wall thickness of ~7 nm. Also, some large pore domains (~6 nm in size) of uncoupled gyroidal subframeworks could be observed at the edges of the particles along the [111] direction, analogous to those observed on highly ordered mesoporous CMK-1 carbon casted from KIT-6 mesochannels.[27] A typical high-resolution TEM (HRTEM) image reveals that these nanoarrays are composed of nanocrystalline Co_3O_4. Figure 3c shows lattice fringes with spacing of ~0.245 nm, which

(27) Kruk, M.; Jaroniec, M.; Ko, C. H.; Ryoo, R. *Chem. Mater.* **2000**, *12*, 1961.

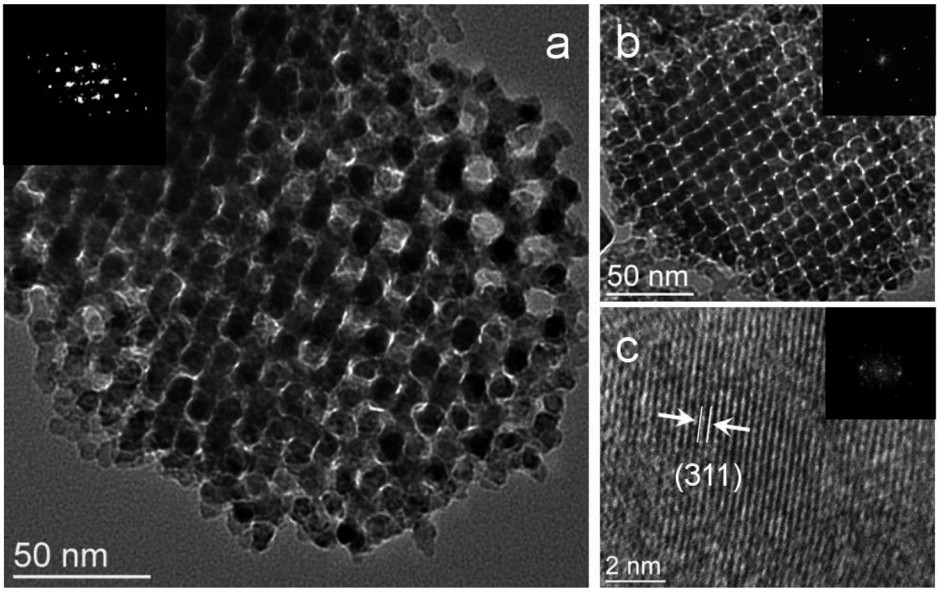

Figure 3. Typical TEM images of cubic mesoporous Co_3O_4/HPW(15) viewed along the (a) [111] and (b) [100] zone axis (possible of the $I4_132$ symmetry). The corresponding fast-Fourier transform patterns are given in the insets. (c) HRTEM image of the mesostructured framework. The two white lines show *d*-spacing of ~0.245 nm, which correspond to the (331) plane of the cubic spinel Co_3O_4 structure.

agrees well with the distance of (311) plane of the Co_3O_4 structure. This indicates that the pore walls are obviously crystalline, as suggested by wide-angle XRD patterns.

The mesoporosity of the replicas is determined by nitrogen physisorption measurements. The N_2 adsorption−desorption isotherms of template-free mesoporous Co_3O_4 and Co_3O_4/HPW(*w*) composites are of type-IV with two H_1-type hysteresis loops, revealing mesoporous property (Figure 4). Such a double hysteresis loop is rarely observed, and it is related to the capillary condensation and evaporation of nitrogen in mesoporous domains with different pore size. The mesoporous Co_3O_4 has a Brunauer−Emmett−Teller (BET) surface area of 141 m^2g^{-1} and total pore volume of 0.25 cm^3g^{-1}, while the mesoporous Co_3O_4/HPW(*w*) composites exhibit BET surface areas in the range of 87−119 m^2g^{-1} and pore volumes in the range of 0.22−0.35 cm^3g^{-1}. It can be observed that the surface area of mesoporous composites decreases gradually as the HPW content increases, probably due to the heavy atoms (i.e., W) of HPW clusters that constitute the frameworks. Pore size analysis with the Barrett−Joyner−Halenda (BJH) method indicates a bimodal pore structure with average pore size at ~4 and ~6 nm, respectively (Figure 4). The pore size of about 4 nm reflects the pores left after the dissolution of the silica walls (~ 3.4 nm, see Supporting Information), while the latter (ca. 6 nm) is corresponding to the large pores observed from TEM images (i.e., between a gyroidal subframework). From the BJH pore size and the SAXS lattice parameter, a wall thickness of ~6.7−7 nm is inferred for mesoporous samples, which coincides well with the TEM results. The small decrease of pore wall thickness relative to that expected from the pore size (8.2 nm) of the silica template is attributed to the shrinkage of the cobalt oxide phase during the solidification process or to the observed mesoporous phase

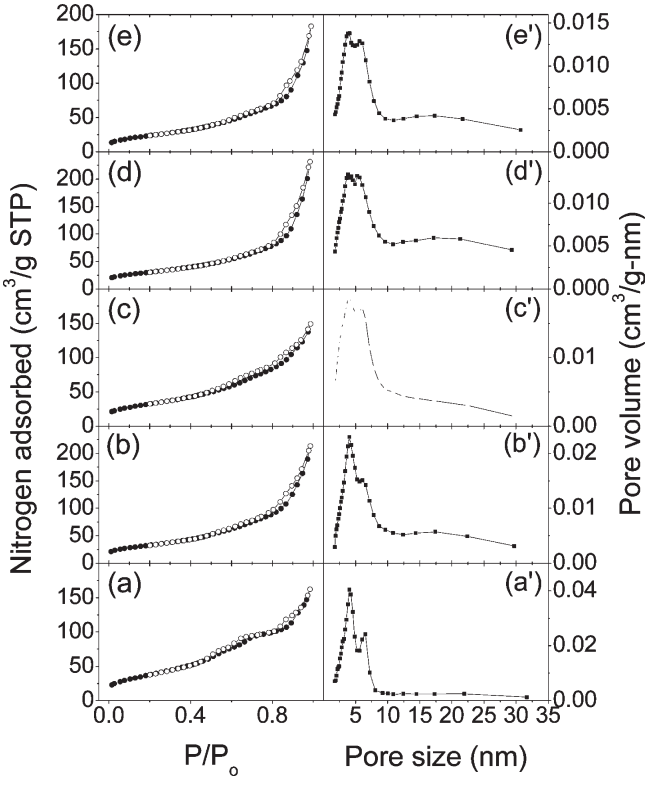

Figure 4. Nitrogen adsorption−desorption isotherms (left) and the corresponding BJH pore-size distributions (right panels) of mesoporous (a) Co_3O_4, (b) Co_3O_4/HPW(6), (c) Co_3O_4/HPW(11), (d) Co_3O_4/HPW(15), and (e) Co_3O_4/HPW(36) samples.

transformation (from $Ia\bar{3}d$ to $I4_132$ or lower symmetry).[28] All textural parameters of mesoporous cobalt oxide and Co_3O_4/HPW(*w*) composites are given in Table 2.

(28) Lu, A. H.; Schmidt, W.; Spliethoff, B.; Schüth, F. *Adv. Mater.* **2003**, *15*, 1602.

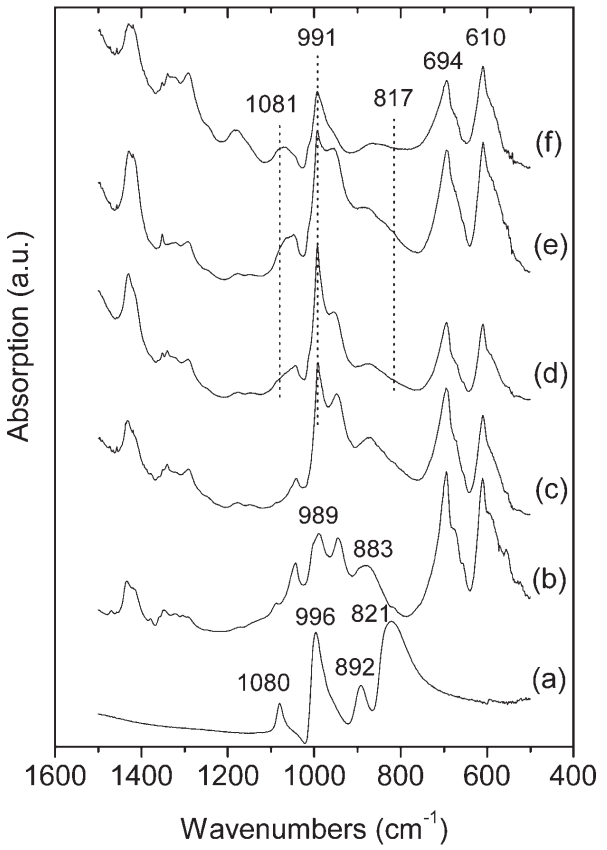

Figure 5. FT-IR spectra of (a) pristine HPW solid and mesoporous (b) Co_3O_4 and (c) Co_3O_4/HPW(6), (d) Co_3O_4/HPW(11), (e) Co_3O_4/HPW(15), and (f) Co_3O_4/HPW(36) composite materials. The strong and sharp absorption peaks at 694 and 610 cm^{-1} are assigned to vibrational modes of Co−O bonds in Co_3O_4 oxide.[31].

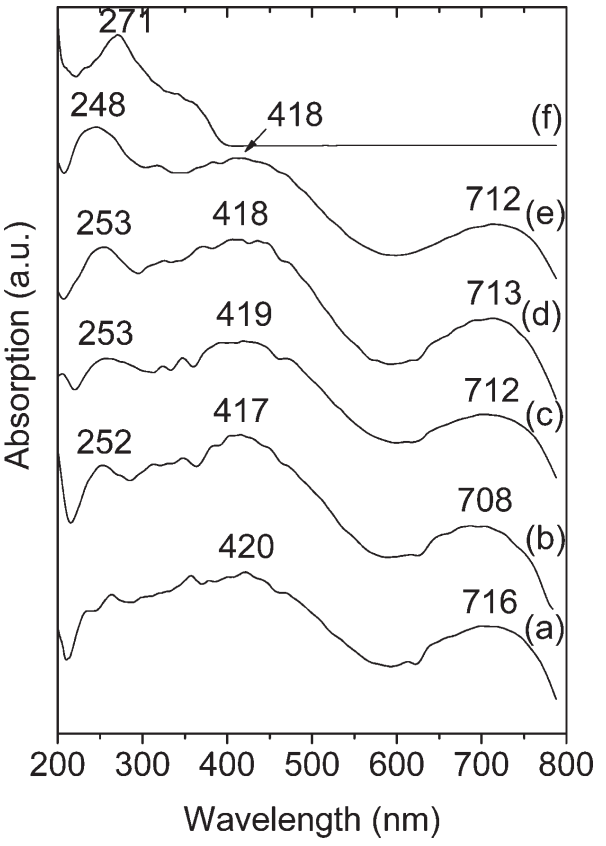

Figure 6. Diffuse reflectance UV/vis spectra of mesoporous (a) Co_3O_4, (b) Co_3O_4/HPW(6), (c) Co_3O_4/HPW(11), (d) Co_3O_4/HPW(15), and (e) Co_3O_4/HPW(36) materials and (f) bulk HPW solid.

The incorporation of HPW clusters into the cobalt oxide network was confirmed with Fourier transform-infrared (FT-IR) and ultraviolet−visible (UV/vis) spectroscopy. The FT-IR spectra of Co_3O_4/HPW(w) composites indicated the characteristic W=O and W−O_c−W (i.e., between the edge-sharing WO_6 octahedra) absorption bands at ~991 and ~817 cm^{-1}, respectively, reflecting the primary Keggin structure of the tungstophosphoric acids in composite frameworks (Figure 5).[29] These absorption bands are red-shifted by ~5 cm^{-1} compared with those of pure HPW, which is attributed to the strong linkage of HPW clusters to the cobalt oxide matrix. The weak absorption band at ~1081 cm^{-1} observed on highly HPW loading samples, Co_3O_4/HPW(w) (w = 11, 15, 36 wt %), is ascribed to the stretching vibration band of P−O bonds in the central PO_4 unit of HPW clusters.[30]

The diffuse reflectance UV/vis spectra of mesoporous replicas shows two intense absorption peaks at ~417−420 and ~712−716 nm, which are assigned to the O(-II)→Co(II) and O(-II)→Co(III) charge-transfer processes in the Co_3O_4 structure (Figure 6).[32] These absorptions are considerably blue-shifted compared to those of bulk Co_3O_4 (~620 and ~828 nm, respectively),[33] possible due to the very small domain size of Co_3O_4 crystallites in these mesoporous frameworks which give rise to quantum confinement effects. The Co_3O_4/HPW(w) composites showed a distinct absorption peak at ~248−253 nm corresponding to the oxygen-to-tungsten charge transfer in W−O bonds of the HPW Keggin clusters. However, these O(-II)→W(VI) absorption peaks are remarkably blue-shifted (~20 nm) compared to bulk HPW (~271 nm),[34] which is consistent with binding of HPW units to the cobalt oxide nanocrystals.

To examine whether the Keggin structure of HPW clusters is preserved intact into the framework, we investigated the local structure of Co_3O_4/HPW(36) sample as well as that of pure Co_3O_4 and HPW compounds with X-ray diffuse scattering and pair distribution function (PDF) analysis.[35] This technique is sensitive to the interatomic distances and can probe the sort-range atomic order of a well-defined structure, such as the crystalline Co_3O_4 and HPW clusters. Figure 7 depicts the PDF plots for mesoporous Co_3O_4 and Co_3O_4/HPW(36) composite materials and pure HPW solid. The PDF plot of mesoporous Co_3O_4/HPW(36) shows strong interatomic correlation

(29) Rocchicciolo-Deltcheff, C.; Thouvenot, R.; Franck, R. *Spectrochim. Acta* **1979**, *32*, 587.
(30) Rocchicciolo-Deltcheff, C.; Gournier, M.; Franck, R.; Thouvenot, R. *Inorg. Chem.* **1983**, *22*, 207.
(31) Gaddsden, J. A. *Infrared Spectra of Minerals and Related Inorganic Compounds*; Butterworth: London, 1975.
(32) He, T.; Chen, D.; Jiao, X.; Wang, Y.; Duan, Y. *Chem. Mater.* **2005**, *17*, 4023.
(33) Cheng, C. S.; Serizawa, M.; Sakata, H.; Hirayama, T. *Mater. Chem. Phys.* **1998**, *53*, 225.
(34) Haber, J.; Pamin, K.; Matachowski, L.; Mucha, D. *Appl. Catal., A: Gen.* **2003**, *256*, 141.
(35) Billinge, S. J. L.; Kanatzidis, M. G. *Chem. Commun.* **2004**, *7*, 749.

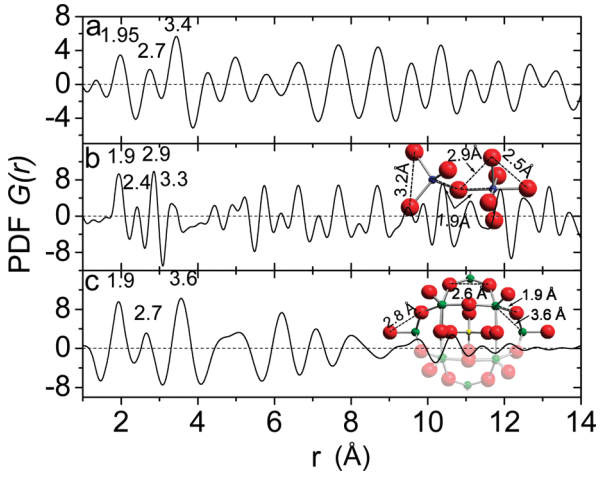

Figure 7. Reduced atomic pair distribution function $G(r)$ as a function of the interatomic distance r for mesoporous (a) Co_3O_4 and (b) Co_3O_4/HPW(36) materials and (c) polycrystalline HPW acid.

vectors at 1.95, 2.7, and 3.4 Å, which ascribed to Co−O and W−O first neighbor, O···O next nearest neighbor, and Co···Co and W···W next nearest neighbor distances of Co_3O_4 spinel and HPW cluster, respectively. It can observed that the PDF plot of Co_3O_4/HPW(36) is a superposition of PDFs of mesoporous Co_3O_4 and pure HPW. These results suggest that the Keggin structure of HPW is retained intact in the cobalt oxide-based framework. The long-distance (> 10 Å) atomic pair correlation peaks of mesoporous Co_3O_4 and Co_3O_4/HPW(36) correspond to the crystalline structure of Co_3O_4.

The chemical state of Co and W atoms in nanostructured frameworks was probed with X-ray photoelectron spectroscopy (XPS). A typical XPS spectrum of Co_3O_4/HPW(15) showed Co $2p_{3/2}$ and $2p_{1/2}$ core-level signals with binding energy at 780.2 and 795.2 eV, respectively (Figure 8a). These binding energies as well as their difference (spin−orbit splitting) at 15 eV are very close to those reported for the mixed valence $Co^{II}Co^{III}{}_2O_4$ compound, implying similar electronic configuration.[32,36] A further indication for the presence of Co_3O_4 phase is the low intensity shakeup satellite at ~9.5 eV from the main spin−orbit component (Co $2p_{3/2}$).[37] While the weak shakeup satellite at ~5.6 eV from the main spin−orbit component is attributed to the surface hydroxyl species (i.e., Co−OH).[32,37] The XPS spectrum of the W atoms shows W $4f_{7/2}$ and $4f_{5/2}$ core-level signals with binding energies at 35.0 and 37.1 eV, respectively (Figure 8b). These values of binding energies suggest W atoms in their higher oxidation state (W^{VI}).[38] A quantitative analysis from XPS data indicates an atomic ratio between the Co and W atoms close to 93.9:6.1, which is consistent with a percentage

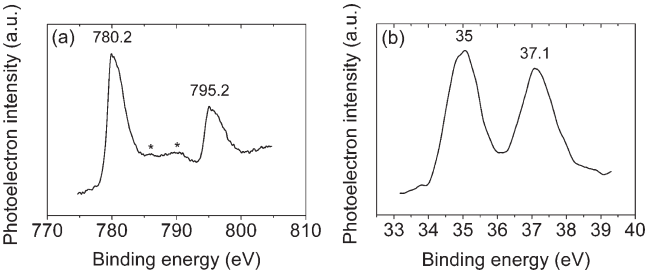

Figure 8. High-resolution (a) Co $2p_{3/2}$ and $2p_{1/2}$ and (b) W $4f_{7/2}$ and $4f_{5/2}$ core-level photoelectron spectra of mesoporous Co_3O_4/HPW(15) composite. The symbols show the shakeup satellites ~5.6 and ~9.5 eV above the main spin−orbit component.

Table 3. Catalytic Conversion of N_2O over Mesoporous Co_3O_4 and Co_3O_4/HPW(w) Materials at 400 °C[a]

material	10^{-4} TOF[b] (s^{-1})	conv. of N_2O (%)	apparent activation energy (kJ mol^{-1})
HPW		< 1	
Co_3O_4	45.0	41.9	102
Co_3O_4/HPW(6)	65.1	58.1	98
Co_3O_4/HPW(11)	45.3	37.7	105
Co_3O_4/HPW(15)	34.8	27.4	102
Co_3O_4/HPW(36)	56.3	33.5	104

[a] Reaction conditions: 10 vol % N_2O in He, 1 atm, W/F = 0.1 g·s/mL, and GHSV ~ 70 000 h^{-1}. [b] Turnover frequency: mol of N_2O converted in time t per mol of Co_3O_4.

of HPW loading at 16.4 wt %, in very good agreement with EDS results.

Catalytic Decomposition of Nitrous Oxide. The title materials were tested for catalytic decomposition of nitrous oxide (N_2O). The N_2O is a strong greenhouse gas since it contributes significantly to the global warming with a potential ca. 300 times greater than carbon dioxide and is involved in the depletion of ozone in the stratosphere.[39] Taking into consideration that emission of nitrous oxide from both natural sources and human activities (e.g., nitric and adipic acid plants) continuously increases, the direct catalytic decomposition of N_2O into N_2 and O_2 is a very attractive solution. Table 3 summarizes the results from N_2O conversion on pure HPW acid and a series of mesoporous Co_3O_4 and Co_3O_4/HPW(w) samples under high space velocity, GHSV ~ 70 000 h^{-1}. Compared to pure HPW and mesoporous Co_3O_4, the Co_3O_4/HPW(w) composites exhibited improved catalytic performance, as indicated from the total conversion of N_2O and the specific activity per mol of catalyst (turnover frequency, TOF; Figure S4, Supporting Information). Indeed, the Co_3O_4 catalyst loaded with ~6 wt % of HPW reaches the highest catalytic activity at 400 °C (N_2O conversion ~58% and TOF ~ 65×10^{-4} s^{-1}). It is worth noting that the Co_3O_4/HPW(w) composites exhibited comparable or even higher TOF than other high-performance catalysts for this reaction such as the Au/Co_3O_4 (~$12.5-75.6 \times 10^{-4}$ s^{-1})[40] nanocomposites and the iron-doped zeolites Fe-ZSM-5

(36) Jimene, V. M.; Fernandez, A.; Espinos, J. P.; Gonazlez-Elipe, A. R. *J. Electron Spectrosc. Relat. Phenom.* **1995**, *71*, 61.
(37) (a) Estrada, W.; Fantini, M. C. A.; de Castro, S. C.; Polo da Fonseca, C. N.; Gorenstein, A. *J. Appl. Phys.* **1993**, *74*, 5835. (b) Jimenez, V. M.; Espinos, J. P.; Gonzalez-Elipe, A. R. *Surf. Interface Anal.* **1998**, *26*, 62.
(38) Chastain, J.; King, R. C. Jr. *Handbook of X-ray Photoelectron Spectroscopy: A Reference Book of Standard Spectra for Identification and Interpretation of XPS Data*; Physical Electronics: Eden Prairie, MN, 1995.
(39) (a) Rodhe, H. *Science* **1990**, *248*, 1217. (b) Ravishankara, A. R.; Daniel, J. S.; Portmann, R. W. *Science* **2009**, *326*, 123. (c) Dameris, M. *Angew. Chem., Int. Ed.* **2010**, *49*, 489.
(40) Yan, L.; Zhang, X.; Ren, T.; Zhang, H.; Wang, X.; Suo, J. *Chem. Commun.* **2002**, *8*, 860.

($\sim$4.7−48.6 $\times$ 10^{-4} s^{-1}).[41] These results indicate that, whereas, the HPW acids are inactive in decomposition of N_2O, however, their incorporation in the Co_3O_4-based nanostructure promotes the catalytic activity, probably by engaging in specific interactions with the cobalt oxide matrix. Here, the incorporated HPW clusters might have a co-operative effect with Co ions (possible via W−O−Co interactions) to form highly active sites for N_2O conversion, or they can act as reactant transfer agents by adsorbing N_2O species. However, this is not clear, and additional work is needed to elucidate the role of HPW on these materials in N_2O decomposition processes. Also, the facile transportation of reactants and products through the ordered pore structure and the large efficient surface area are other significant factors that contribute further to catalytic performance of this system.

Conclusions

In conclusion, the synthesis of highly ordered mesoporous frameworks constituted by nanocrystalline Co_3O_4 and tungstophosphoric acid clusters through a hard templating method has been demonstrated. The obtained composite materials feature a Co_3O_4/HPW solid solution structure in cubic packed symmetry. Preliminary catalytic studies have indicated that such Co_3O_4/HPW composites can be effective catalysts, exhibiting exceptional catalytic activity on direct decomposition of N_2O. We believe that the present approach can be extended to other mesoporous nanocomposites with different metal-oxide and polyoxometalate acid components. These mesoporous materials are expected to have great implication in various fields of catalysis, including combustion of pollutants and partial oxidation of hydrocarbons.

Acknowledgment. This work was supported by European Community under a Marie Curie International Reintegration Grant (No. 230868). We thank Dr. C. Malliakas (NU) for help with handling the PDF data.

Supporting Information Available: SAXS patterns and N_2 adsorption−desorption isotherms of mesoporous KIT-6, SEM-EDS spectra of mesoporous Co_3O_4 and Co_3O_4/HPW(36) samples, and catalytic profiles of mesoporous Co_3O_4 and Co_3O_4/HPW(*w*) composite materials (PDF). This material is available free of charge via the Internet at http://pubs.acs.org.

(41) Pèrez-Ramirez, J.; Kapteijn, F.; Mul, G.; Moilijn, J. A. *Chem. Commun*. **2001**, *8*, 693.